Journal of Applied Mechanical Engineering
ISSN: 2168-9873

Mondal et al., J Appl Mech Eng 2017, 6:6
DOI: 10.4172/2168-9873.1000291

Research Article Open Access

Effect of Strain Rate and Relative Density on the Compressive Deformation of Open Cell Ti_6Al Alloy Foam through P/M Route

Mondal DP[1]*, Barnwal AK[1] and Diwakar V[2]

[1]CSIR-Advanced Materials and Processes Research Institute, Bhopal, India
[2]University Institute of Technology, Barkatullah University, Bhopal, India

Abstract

Open cell Ti_6Al alloy foams of varying porosity fractions have been made using ammonium bicarbonate as space holder through powder metallurgy route. In order to provide the sufficient strength in green compacts 2% of wt.% PVA solution was mixed with elemental metal powder and $NH_4(HCO_3)$ particle prior to cold compaction. Green pallets were sintered at three stages at three different temperatures 600°C, 800°C and 1100°C. XRD and EDX analyses confirmed that no residue of space holder remained in the sintered foam samples. The compressive deformation behavior of Ti_6Al alloy foams with varying relative densities was conducted under different strain rates (0.01, 0.1, and 1.0 s^{-1}). The plateau stress, the Young's modulus and the energy absorption of the foam increase with increase in the relative density following power law relationships. But the densification strain decreases with increases in relative density following a linear relationship. The strain rate sensitivity and the strain rate sensitivity parameter of these foams were also examined, and it was found that the strain rate sensitivity parameters were varying in the range 0.034 to 0.078.

Keywords: Ti-Al alloy foams; Sintering; Compressive deformation; Plateau stress; Energy absorption; Strain rate sensitivity

Introduction

Open cell titanium alloy foam plays a vital role in the biomedical science and technology. This is primarily special for orthopedic and dental implants, skeletal repairing and osseointegration [1], due to its biocompatibility, tailor made specific strength, and superior corrosion resistance in bio-fluid and compatible with MRI imaging. Some of the metal foams are also used as energy absorbers, filters, gas distributor and heat exchanger [2]. Titanium and its alloy have high strength at elevated temperature and thus can be used for filters, energy absorption components, catalyst substrate at high temperature.

For bone implantation in human body, some problems are associated with implant materials. These are stress shielding effect, body fluid flow, substantial bone growth, and tissue growth [3]. To avoid the stress shield effect, the implant and bone material should have almost same modulus and strength. The modulus of titanium foam can be tailor made to that of bone though adjustment of volume fraction and size of porosities. The modulus of human bone is 10-30 GPa [4,5]. Solid titanium alloys have Young's modulus (80-110 GPa) which is much higher than that of human bone. By varying the porosity in the range of 40-70%, its modulus can be matched with that of human bone [6]. For substantial bone growth, pore size requirement is 100–600 μm and un-mineralized asteroid tissue in growth pore size requirement is 75-100 μm. On the other hand, for fibrous tissue growth it is 10-75 μm [7,8]. The pore size and volume fraction of pores should be controlled to control the mechanical properties and bone microstructure [9] as well as tissue in growth.

Making Ti-foams by liquid metallurgy route is difficult. Because, (a) titanium has high melting point (approximately 1678°C), (b) at high temperature, titanium has high chemical affinity to react with atmospheric gasses such as oxygen and nitrogen because of incomplete electron shell [10]. Because of these limitations, other methods like (i) powder metallurgy (P/M) and (ii) metal ion and metal vapor deposition technique [11,12] are used for making Ti foam. In case of powder metallurgy, porosity in metal is created using different methods such as loose powder sintering [13], gas entrapment method [14], replication method [15] and space holder method (the sintering of matrix alloy powder and space holder powder mixture after cold compaction) [5]. The porosity and pore size of metallic foam could be controlled by the control of amount of space holder material and its particle size of space holder [16]. Some materials like NaCl [17], saccharose [18], carbamide [19], magnesium [20], ammonium bicarbonate [16,21] were used as space holder.

For bone-implant purpose, number of Ti-alloy foams was developed which provide favorable environments for new bone growths and body fluid flow within the artificial bones [9,16,17]. As per requirement of bone implant applications in different locations, titanium based alloy foam such as, Ti-34Nb-29Ta-xMn (x: 2%, 4%, 6% wt. Mn) with porosity of 45-50%, Young modulus of 30 GPa and pore size of 165-230 μm were made with space holder technique [22]. Finally sintering was done, where in the sintering temperature were varied to get varying mechanical properties [22]. In another report Ti_6Al7Nb foam with porosity of 70%, pore sizes of 200 μm are made using cold compact pressure of 500 MPa [23]. The Ti_6Al4V foam with porosity of 51-65% exhibited Young modulus of 4-12 GPa as reported by Asik et al. [24]. Ti-50.8 Ni foam with porosity 39-58% was made using magnesium as space holder by Nakas et al. [25] exhibited young modulus 5.87-12.49 GPa. This Ti-Ni foam during cold compaction a pressure of 250-600 MPa was used. Munoz et al. [26] also made an attempt to make Ti foam with porosity of 70% and pore size of 165-230 μm, using cold compaction pressure of 800MPa and sintering temperature of 1200°C where ammonium bicarbonate was used as space holder. The present author has also made attempts, for making Ti-foam using NaCl

***Corresponding author:** Mondal DP, CSIR-Advanced Materials and Processes Research Institute, Bhopal-462026, India, Tel: +91-755-2488562; E-mail: dpmondal@ampri.res.in

Received September 26, 2017; **Accepted** October 23, 2017; **Published** October 27, 2017

Citation: Mondal DP, Barnwal AK, Diwakar V (2017) Effect of Strain Rate and Relative Density on the Compressive Deformation of Open cell Ti_6Al Alloy Foam through P/M Route. J Appl Mech Eng 6: 291. doi: 10.4172/2168-9873.1000291

[17], Acrowax [9] and ammonium bicarbonate [16] as space holder to get porosity in the range of 40% to 70%. They examined that the space holder also affects the mechanical properties [16]. The strength and modulus of foam also varied with particle shapes [9]. The Ti-alloyed foams were made primly using by milled alloy powder [27]. Limited attempts are made to make Ti-alloy foams using elemental powder [22-25]. To the best of our knowledge, so far no attempt has been made to make Ti_6Al alloy foam using elemental powder and ammonium bicarbonate as space holder. As aluminum melt at lower temperature, it has greater possibility for diffusion during sintering at high temperature (500-600°C). If Ti-Al mixture is directly heated at temperature greater than 700°C, there is possibility of drainage of Al without diffusion in Ti. In view of that sintering of elemental powder mixture to foam alloy is difficult. This paper deals with preparation of Ti-Al alloy foams at different porosity fraction using elemental powder of Ti, Al and ammonium bicarbonate as space holder. Finally, the foam is characterized in term of microstructure. The strain rate sensitivity of this foam was also examined. Our body work at dynamic condition and there is a need to examine the strain rate sensitivity of these foam. In view of this, this paper also deals with the effect of strain rate on its deformation behavior and to examine the strain rate sensitivity and the sensitivity parameter as a function of foam relative density

Experimental Procedure

Raw materials

Titanium and aluminum powder (purity 99.9%) supplied by Alfa Aesar have been used as matrix, raw material for the average particle sizes of titanium and aluminum powder were 25.2 ± 2.1 μm and 14 ± 1.8 μm respectively. Here ammonium bicarbonate was used as space holder. The average size of ammonium bicarbonate was 230 ± 15 μm. Ammonium bicarbonate powder was also supplied by Alfa Aesar, UK. A PVA solution (5 wt.% PVA and 95% water) was used as an organic binder to provide sufficient strength to cold compacted green pallets. The elemental powders of Ti and Al were in angular in shape, whereas ammonium bicarbonate powders were cubic in shape.

Foam production

Ti-Al alloy powder were mixed with space holder ($NH_4(HCO_3)$) in different proportion for getting varying relative densities (0.4, 0.5, 0.6 and 0.7). 2 wt% of PVA solution was added in the metal powder mixture. The mixed powders were cold compacted using 200 MPa pressure in a hydraulic press of capacity 40 ton. Cylindrical samples of 15 ± 1 mm diameter and 10 ± 0.2 mm height was made. Varying amount of Ti-Al alloy powder and $NH_4(HCO_3)$ used for obtaining different porosity level, were calculated through the following relationship [14].

$$\frac{w_{tap}}{W_{sp}} = \frac{\rho tap^{*}\left(1-V_{sp}\right)}{\rho_{sp}{}^{*}V_{sp}} \quad (1)$$

Where W_{tap} represents the weight of the titanium alloy powder, W_{sp} denotes the weight of space holder and V_{sp} represent the volume fraction of space holder. Green pallets were dried at 200°C for 2 hours to evaporate out ammonium bi-carbonate. During drying, moisture as well as $NH_4(HCO_3)$ and PVA get removed. These green pallets were then heated at 400°C for 1 hour. Finally, these are sintered at three different stages at three different temperatures (600°C, 800°C and 1100°C) for 1 hr. at each stage under high vacuum (10^{-4} mbar). The flowchart for making these foams and the sintered foam samples are shown in Figures 1a and 1b respectively. During sintering the heating rate is maintained at 2°/s in order to avoid thermal stress which may cause cracking of sintered sample.

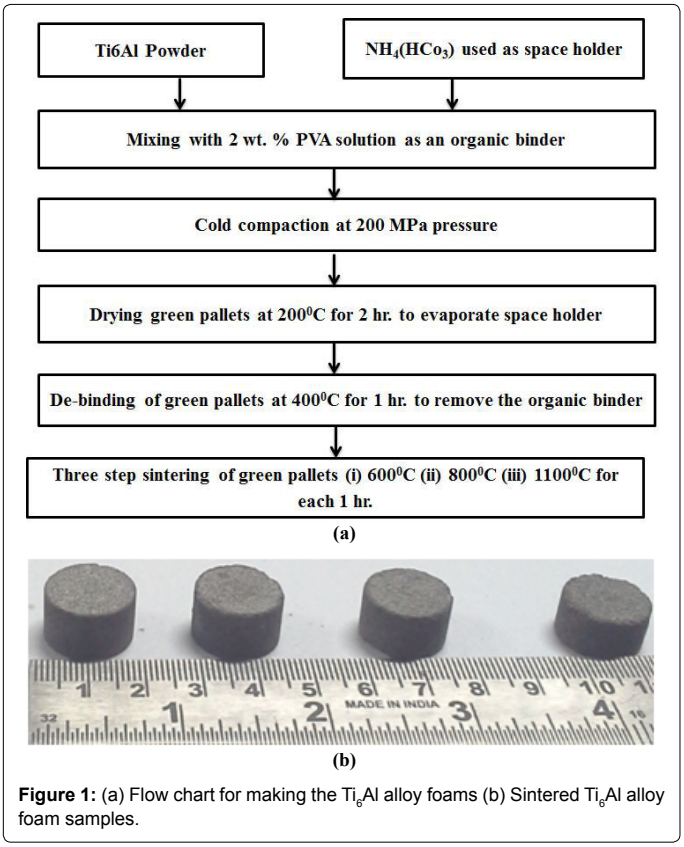

Figure 1: (a) Flow chart for making the Ti_6Al alloy foams (b) Sintered Ti_6Al alloy foam samples.

Microstructure characterization

The pallets of sintered Ti_6Al alloy foam were examined using scanning electron microscopic (SEM) (JEOL; Model: 5600). Firstly at least 150 cells and cell walls were selected randomly in SEM micrographs. The cell sizes and cell wall thicknesses of individual cells of the micrographs were noted, and then computed to get the average apparent cell size and cell wall thickness. The true value of cell size and cell wall thicknesses were then measured by comparing the scale recorded in the micrographs. X-ray diffractometer (Model: Bruker-D8 with Cu_α radiation) was used to find out physical and chemical changes in phase constituents and residues left in the foam after sintering, at a scan rate of 0.01°. The EDX analysis of the overall foam and its cell wall were also carried out to confirm the chemistry of foam using EDX system (model: IE synergy 250) attached with the Field Emission Electron Microscopic (FESEM) (Model: Nova-Nano SEM 430).

Compression test

Compression test of cylindrical samples (15 ± 1 mm diameter and 10 ± 0.2 mm height) were performed in a universal test machine (UTM) (Instron: 8801) at room temperature under varying strain rates (0.01, 0.1, 1.0 s^{-1}). These tests were repeated thrice for each category of sample. Prior to compression test, the specimen surface were made flat and covered with MOS_2 to reduce fraction between specimen and plate surface. The compressive stress strain curves along with data were recorded during testing. All these recorded data are used to plot the graph between compressive stress and compressive strain using standard methodology [9,16,17,21]. The Young modulus, the plastic collapse stress, the plateau stress, the densification strain and the

energy absorption are calculated with the help of compressive stress and strain diagram of Ti_6Al alloy foam as a function of relative density and strain rate. The data obtained from the compressive strain curves were used for calculating the plastic collapse stress, plateau stress, densification strain, energy absorption, strain rate sensitivity and strain rate sensitivity parameter.

Results and Discussion

Material and microstructure

Figure 2 represents the microstructure of Ti_6Al foam with varying relative densities (RD). It is evident from these Figures (Figures 2a-2d) that the cell size is almost invariant to the relative density. But, the cell wall thickness decreases with decrease in relative density. The cell size and cell wall thickness were measured from these types of micrographs using the methodology as stated elsewhere [24]. The average cell size and cell wall thickness along with standard deviation were reported in Table 1. The higher magnification micrographs of Ti_6Al foam are shown in Figures 2e and 2f for relative density of 0.26 and 0.39 respectively. It is evident from these Figure that the cell wall contains finer micro porosities (marked arrow), in addition to the micro pores due to evaporation $NH_4(HCO_3)$. The cause of formation of micro pores is the interstitial voids among the titanium particles. Here, the sintering is carried out at 1100°C, it is expected that the Ti-Al alloy particles will not be fused. But large extents of solid state diffusion take place. This causes good bonding among the particles and alloying with aluminum. Figure 2g reveals that metallic particle after solid state diffusion bounded with each other and formed grain structure (noted 'g'). It further reveals inter connectivity with neighbor cells (marked 'C') which can allow fluid to flow.

Relative Density	Cell Size (μm)	Cell Wall Thickness (μm)	Aspect Ratio
0.26	224.39 ± 10	23.390 ± 2	1.23
0.33	219.72 ± 10	39.036 ± 4	1.21
0.39	217.00 ± 10	105.30 ± 8	1.19
0.46	216.00 ± 10	359.87 ± 10	1.17

Table 1: Average cell size, cell wall thickness and relative density.

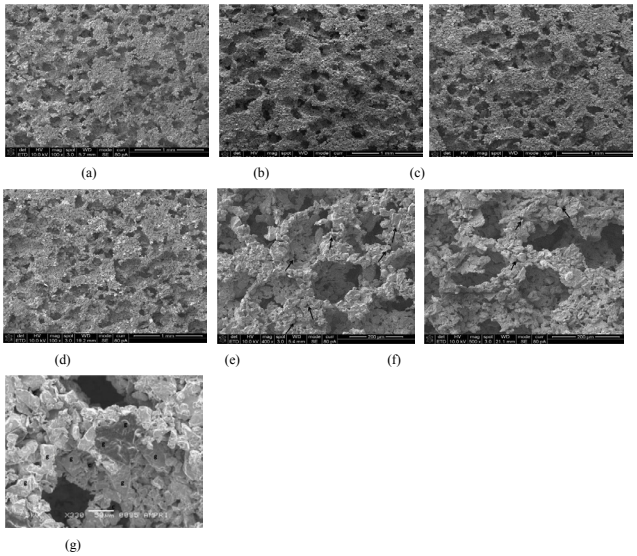

Figure 2: Micro-structures of TI6Al alloy foam samples are (a) relative density of 0.26, (b) relative density of 0.33, (c) relative density of 0.39, (d) relative density of 0.46, (e) higher magnification with relative density of 0.26, (f) higher magnification with relative density of 0.39, and (g) higher magnification with relative density of 0.39.

It is evident from Table 1 that the average cell sizes in these foams are varying in the range of 216 to 224 μm. This is almost similar to the average size of space holder (230 μm). It proves that the space holder size is primarily responsible for the formation and control of the cell size. By controlling the space holder here, the cell size can be controlled. Only marginal decrease in cell size is noted as compared to the average space holder size. This is because of the two counter phenomena, which took place during sintering. Due to sintering there is a possibility of shrinkage due to closure of few inter particle pores in the cell wall through solid state diffusion among the metallic particles. A large extent of pores is existing within the cell wall in between the metallic particles in the green pallets. Only a few of them get annihilated during the sintering. As a result, the overall shrinkage of cells is almost negligible. The cell wall thickness increases with relative density. This is primarily due to the fact that the solid fraction is increasing, and the solid metals are being occupied on the cell wall. As less amount of space holder was used, the inter-space holder distance, which built the cell wall, increases. This results in thicker cell wall at higher relative density.

EDX and X-RD analysis

The EDX analysis of the foams samples was carried out to investigate the elemental distribution in the foam. The microstructures along with elemental distribution in the foams with relative densities of 0.26 are shown in Figure 3a. It is evident from Figure 3a that titanium is present, in general in the major amount. It is noted that both titanium and aluminum are distributed uniformly within the cell wall. These signify that Ti and Al have been alloyed uniformly. Similar observations are made in Figures 3b and 3c for relative density of 0.33 and 0.46, where more amounts of Ti and Al are used. These are also uniformly distributed within the cell wall and indicate effective alloying of Al in Ti. XRD analysis was performed on the sintered foam sample as shown in Figure 4. It does not show any peak corresponding to Al. This confirmed that Al get diffuse into Ti and formed intermetallics of Ti_6Al or Ti-base solid solution. Peaks for intermetallics compounds like Ti-Al, Al_3Ti, and $AlTi_3$ are observed. These intermetallics phases are formed due to solid state diffusion between Ti and Al within the alloy matrix. In addition to the intermetallics phases, peaks for Ti are also present, indicating formation of Ti-Al solid solution.

Sintering temperature and relative density

The porosity increased with decrease in RD. The relative densities (RDs) of foam before and after sintering are compared in bar chart as shown in Figure 5. It is evident from this Figure that RD of foams increases after sintering. The value of RD of sample after sintering was increased due to (a) solid state diffusion; (b) softening of metallic powder and (c) filling of inter particle voids by Ti-Al alloy. In our study, sintering process was carried out through step sintering because of the use of aluminum as alloying element in titanium. If we were going to sinter directly at 1100°C all the aluminum would have been melt out and leave its position in sample without alloying. In 600°C aluminum are diffused in titanium and at this temperature solid state sintering happened between aluminum and titanium particles. At 800°C aluminum particle filled few of the voids or gap between titanium particles and diffuse fully within titanium to form α-Ti and Ti_3Al phase. According to the phase diagram, above 930-940°C, Ti_6Al started phase transformation from α (HCP) to β (BCC structure). At temperature 1100°C, when it hold for 1 hr Ti_6Al alloy get sintered and transformed into β-Ti. The samples after sintering are cooled to room temperature

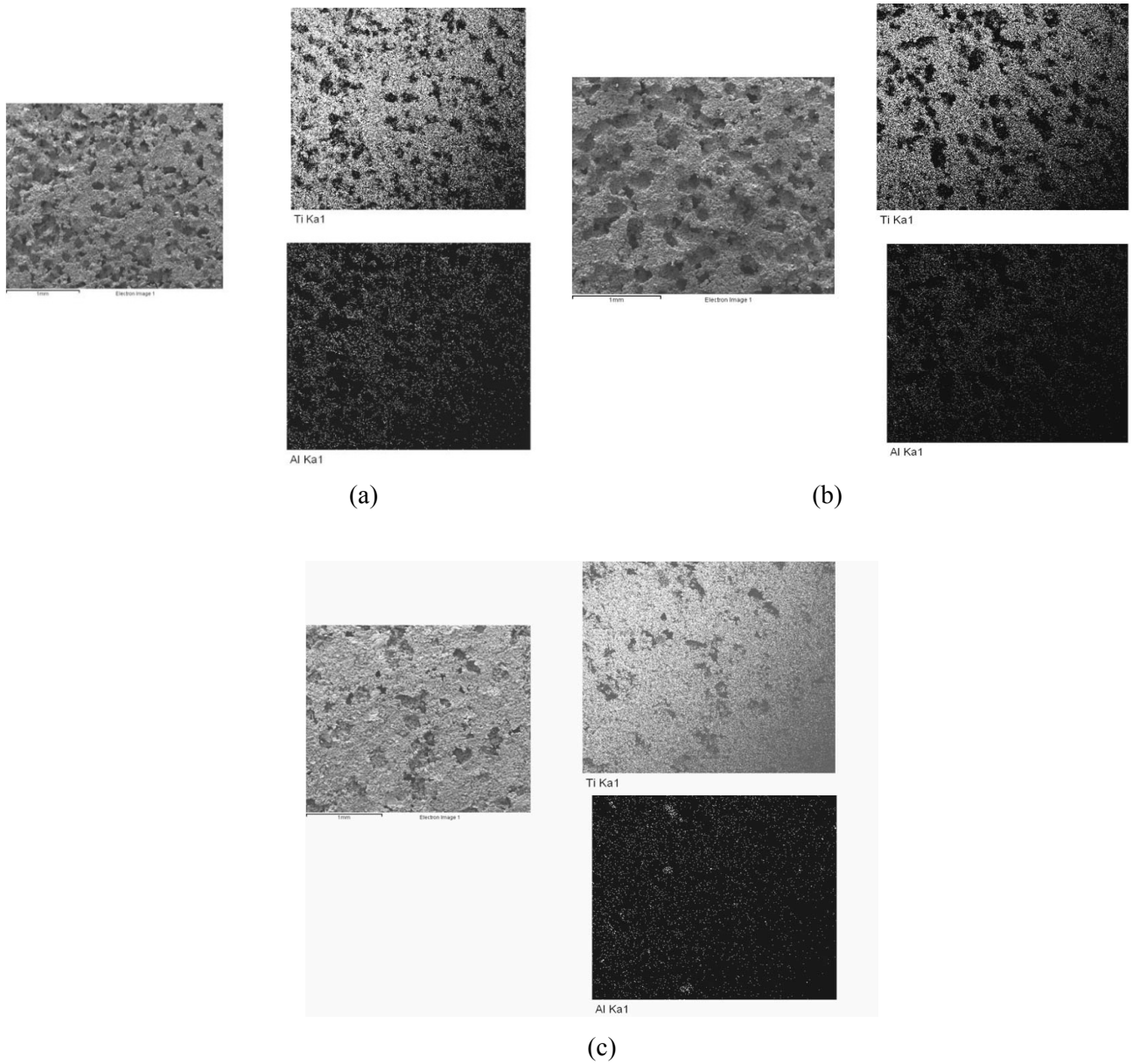

Figure 3: Elemental distributions of Ti6Al alloy foam samples are (a) Relative density of 0.26, (b) Relative density of 0.33, and (c) Relative density of 0.46.

at a cooling rate of 2°/minutes. During cooling, β-Ti transfer to α-Ti + Ti_3Al. This is exactly observed through XRD (Figure 4). Because of these reasons, a fraction of micro pores get annihilated and shrinkage in the sample is noted. This causes reduction in porosity and increase in relative density. The alloy also get soften and there is a possibility of micro-deformation on the cell wall causing shrinkage of cell size marginally. In view of the understanding of these facts, the density of foams after different stage of heating are examined and shown in Table 2. It is evident from this Table 2 that the relative density increased very marginally after heating at 600°C. But after heating at 800°C, relative density increase to a large extent (by 5%). However after sintering at 1100°C the relative density increases by 10-12%. This signifies that that solid state diffusion and softening of the diffused alloy took place primarily at 1100°C and leading to reduction in porosity as well as cell size, which, in other words, causing higher relative density. Because of the presence of more metallic material, which is subjected to sintering, the extent of shrinkage after sintering is higher leading to increase in relative density to a greater extent, at higher relative density. Even though the fraction of porosity get annihilated during sintering, the absolute value of porosity annihilated will be more, leading to greater extent of reduction in porosity and increase in shrinkage, at higher density of foam material.

Compressive deformation

The compressive stress strain curves of Ti_6Al foams with different relative densities are at fixed strain rate of 0.01 sec^{-1} shown in Figures 5 and 6. It is clearly observed from these Figures that the stress-strain curves have distinctly three regions (i) linear region i.e., where stress is directly proportional to strain; (ii) plateau region (stress remains almost unchanged with strain) and (iii) densification strain (stress increases

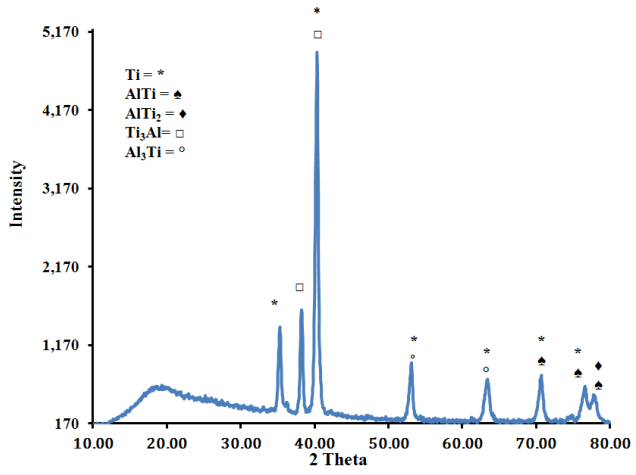

Figure 4: XRD pattern of sintered Ti-$_6$Al alloy foam.

Relative Density	Increase of relative density after the sintering at different stage %		
	600°C	800°C	1100°C
0.26	2.1	5.0	10.1
0.33	2.0	5.2	11.4
0.39	2.5	5.5	12.3
0.46	2.4	5.5	12.8

Table 2: Shrinkages after each stage of sintering.

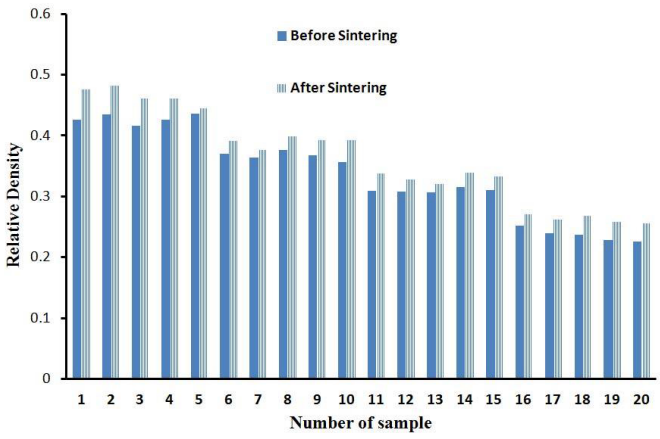

Figure 5: Effect of relative density of Ti_6Al alloy foam samples on before and after sintering.

rapidly with slight increase in strain). The stress-strain curve of these Ti_6Al foams is similar to that of other metal foam [21]. The plateau stress and densification strain of Ti_6Al foam is determined from these stress strain curves and reported that Table 3 using the methodology as stated elsewhere [9,28]. It is also noted from this Figure that the stress increases to a peak value and then reduced to plateau level and these stress increases with increase in relative density. This is due to increase amount of solid fraction which is responsible for carrying the load in the foams. The slope of linear regions also increases with increase in relative density. That indicated the modulus increases with increase in relative density. But densification strain decrease with increase in RD. This is due to less amount of porosity in the foam with higher relative density. It is further noted that the nature of stress strain curves almost invariant to the RD. In general, it is observed that after yielding, there is a stress drop to reach the plateau region. The peak stress after yielding is considered as plastic collapse stress. The stress drop ratio defines as the ratio of stress drop to the plastic collapse stress. The compressive stress strain curves of the sintered foam having relative density of 0.26 for different strain rates are shown in Table 3. The natures of stress-strain curve are similar to that observed in Figure 6 and the nature is almost similar at all strain rates. But stress drop ratio increases with increase in strain rate. It is future noted that the plastic collapse stress, plateau stress increases with increase in strain rate. It is also interesting to note that the densification starts earlier in case of higher strain rate. This may be due to greater thrust of loading at higher strain rate which causes early facture of cell wall but at higher stress value. These stress strain curve for all the materials tested are used for determining plateau stress, plastic collapse stress, densification stress, energy absorption and the average of these a function of relative density and strain rate are reported in Table 3.

Plateau stress

The plateau stress (σ_{pl}) of Ti_6Al alloy foam as a function of RD at different strain rates is shown in Figure 7. It is depicted from this Figure that σ_{pl} increases with increases in relative density and follow the power law relationship like other foam [2,20,28-33]. The coefficient and exponential for the best fitted power law relationship are also reported

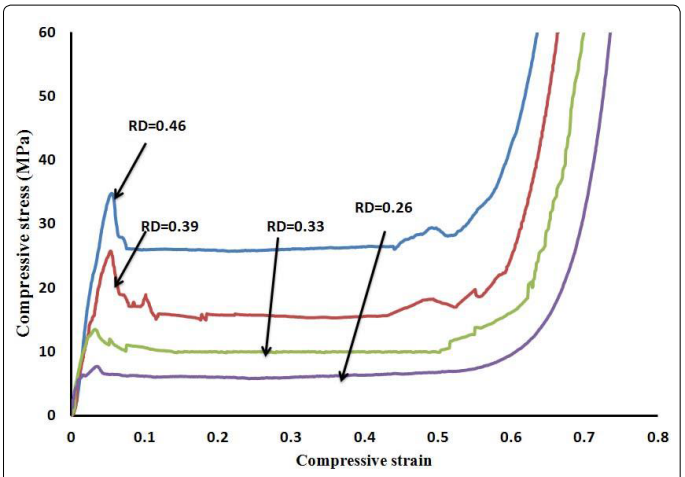

Figure 6: Compressive stress strain curves of Ti_6Al foams at constant strain rate of 0.01/s with different relative density.

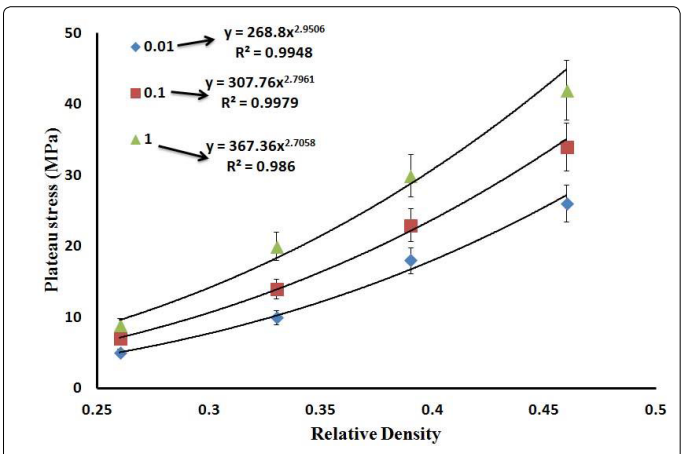

Figure 7: Variation of plateau stress (σ_{pl}) of Ti_6Al alloy foam with relative density.

Relative Density	Strain Rate/s	σ_{pl} (MPa)	E (GPa)	ε_D	E_{ab} (MJ/m³)	σ_q	σ* (MPa)	σ_d (MPa)	$(\Delta\sigma/\sigma_{p1})$	∑
0.26	0.01	5 ± 0.25	0.9 ± 0.045	0.62 ± 0.031	2.5 ± 0.125	6.3 ± 0.32	6.8 ± 0.34	6.95 ± 0.35	0.5 ± 0.025	0.041513 ± 0.002
	0.1	7 ± 0.35	1.5 ± 0.07	0.63 ± 0.032	3.5 ± 0.175	6.3 ± 0.32	8.2 ± 0.41	9.1 ± 0.45	0.35 ± 0.016	0.074148 ± 0.003
	1	9 ± 0.45	2.1 ± 0.1	0.64 ± 0.032	4.6 ± 0.23	6.3 ± 0.32	11 ± 0.55	12 ± 0.6	0.3 ± 0.015	0.075015 ± 0.003
0.33	0.01	10 ± 0.5	2.5 ± 0.13	0.6 ± 0.03	5.2 ± 0.25	13.23 ± 0.68	12.56 ± 0.62	14.56 ± 0.7	0.25 ± 0.012	0.045988 ± 0.002
	0.1	14 ± 0.7	4.3 ± 0.25	0.61 ± 0.031	7 ± 0.35	13.23 ± 0.68	18.01 ± 0.9	19.12 ± 0.9	0.25 ± 0.012	0.071016 ± 0.003
	1	20 ± 0.1	6.5 ± 0.32	0.62 ± 0.031	9.6 ± 0.48	13.23 ± 0.68	21.86 ± 1.1	24.13 ± 1.2	0.20 ± 0.01	0.072184 ± 0.003
0.39	0.01	18 ± 0.9	5 ± 0.25	0.58 ± 0.03	7.3 ± 0.36	21.86 ± 1.1	22.23 ± 1.1	23.62 ± 1.2	0.41 ± 0.02	0.034384 ± 0.002
	0.1	23 ± 1.2	8.5 ± 0.42	0.59 ± 0.03	10 ± 0.5	21.86 ± 1.1	28.2 ± 1.4	31.24 ± 1.6	0.19 ± 0.01	0.072228 ± 0.003
	1	30 ± 1.5	12 ± 0.06	0.6 ± 0.03	13.5 ± 0.68	21.86 ± 1.1	32.65 ± 1.6	39.48 ± 1.9	0.10 ± 0.005	0.078124 ± 0.003
0.46	0.01	26 ± 1.3	9 ± 0.45	0.55 ± 0.029	11.5 ± 0.56	31.56 ± 1.6	35.62 ± 1.6	35.56 ± 1.9	0.30 ± 0.015	0.04877 ± 0.002
	0.1	34 ± 1.7	14 ± 0.7	0.565 ± 0.029	14.8 ± 0.76	31.56 ± 1.6	39.95 ± 1.9	41.9 ± 2.1	0.17 ± 0.08	0.056203 ± 0.002
	1	42 ± 2.1	18 ± 0.9	0.58 ± 0.029	17.5 ± 0.79	31.56 ± 1.6	42.31 ± 2.1	49.21 ± 2.5	0.25 ± 0.012	0.06039 ± 0.003

Table 3: Mechanical properties for Ti_6Al alloy form.

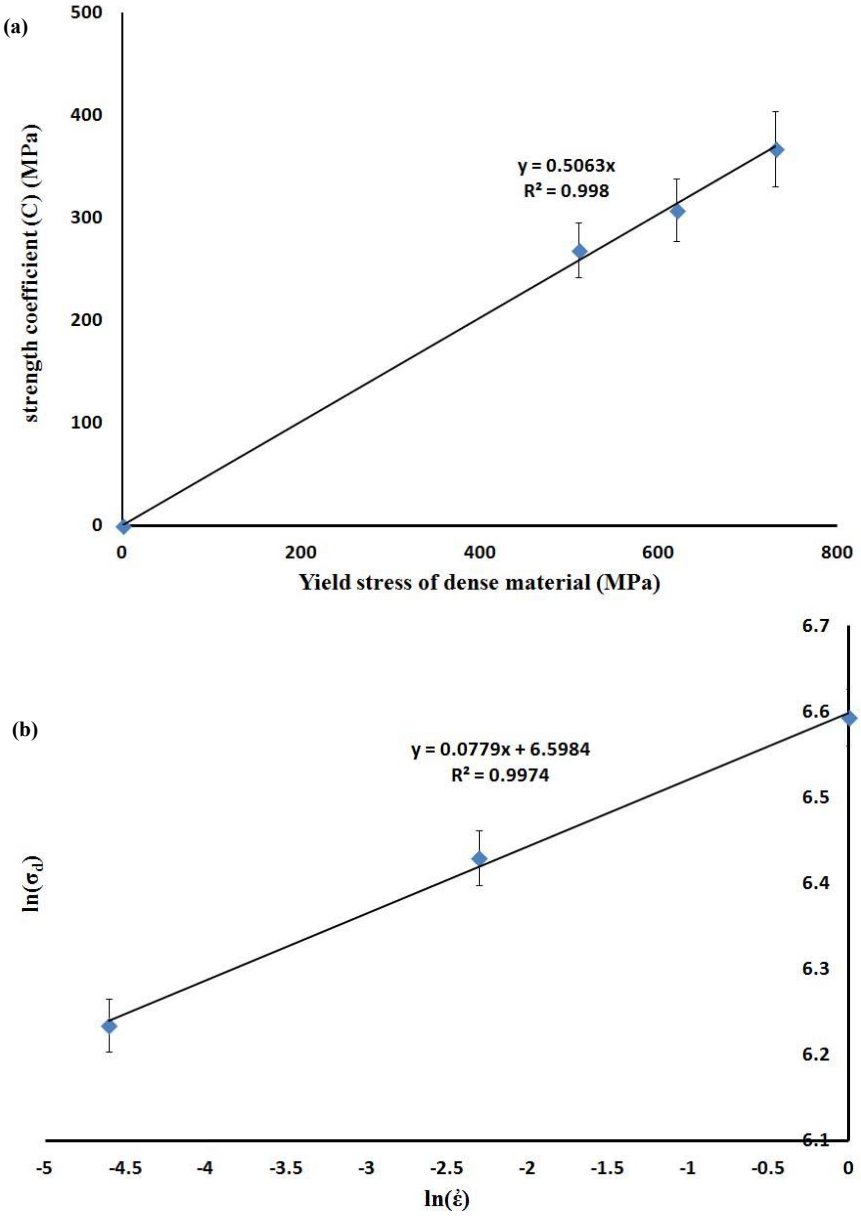

Figure 8: (a) Relation between coefficient (C = c x σ*yd*) and yield stress of dense material (σ*yd*), and (b) relation between ln (σ*yd*) and ln (ε̇).

in Figure 7. It is noted that the plateau stress follow the following type power law relationship.

$$\sigma_{pl} = c \times \sigma_{yd} (\rho_{rd})^n \quad (2)$$

In theoretical model, the value of constant 'c'& exponent 'n' are 0.3 and 1.5 respectively [34]. The Similarly, in order to get the value of c, the compressive deformation of dense Ti_6Al alloy (after sintering) are carried out at different strain rate. The yield stress (σ_{yd}) of dense Ti_6Al were measured to be 510, 620 and 730 MPa at strain rate of 0.01, 0.1 and 1.0 s^{-1} respectively. Figure 8a depicted the relation between coefficient ($c \times \sigma_{yd}$) and Yield stress of dense material (σ_{yd}). The slope of linear fit between these two parameters gives the value of 'c' and it is noted to be 0.5063. The coefficient and exponent for power law relation are compared with the reported value in Table 4. It is noted that these coefficient and exponent obtained in present studies are in good agreement with reported the value. 'C' and 'n' varies with RD and 'ε̇' due to variation on micro-architectural characteristics and deformation response or mechanism of foams with ε̇ and RD.

Figure 8b shows the relation between ln (σ_{yd}) verse ln (ε̇), to find out the relation between σ_{yd} and strain rate. The relation between σ_{yd} and ε̇ can be expressed as eq. (3). Figure 9 depicts the relation between exponential ('n') vs. ln (ε̇) which can be expressed in the form of eq. (4)

$$\sigma_{yd} = 733.91 \times \dot{\varepsilon}^{0.0779} \quad (3)$$

$$n = 2.6958 - 0.0531 \ln(\dot{\varepsilon}) \quad (4)$$

By combining the equations (2), (3) and (4), the plateau stress can

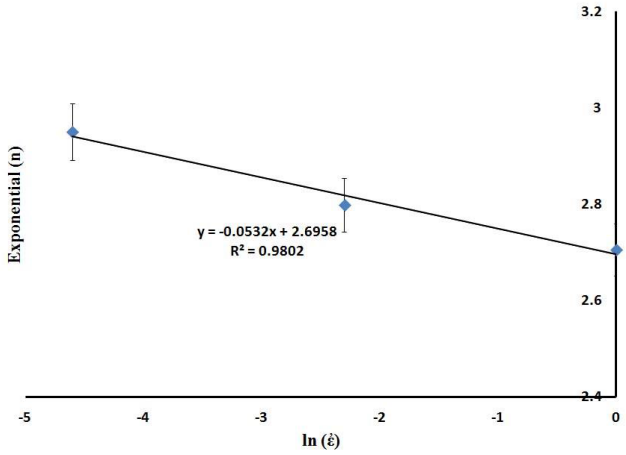

Figure 9: Relation between exponential (n) (of the plateau stress (σ_{pl}) and relative density) verse strain rate (ε̇).

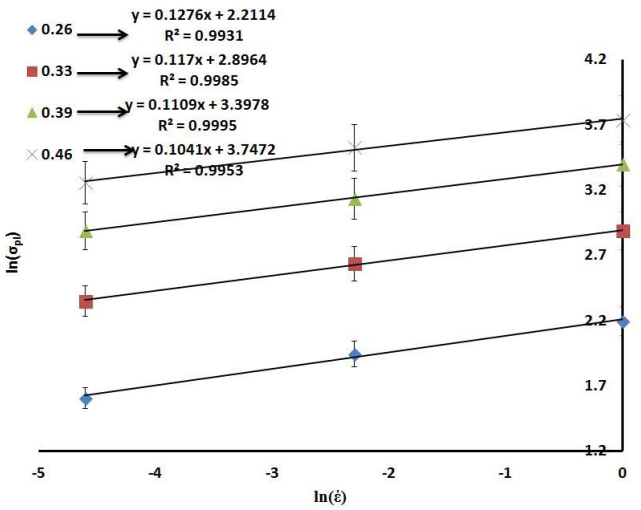

Figure 10: Variation of the ln ($_{pl}$) v/s ln (ε̇) for different relative density.

Equations	C	n	References
$\sigma pl = C * \sigma_d * \left(\frac{\rho_f}{\rho_d}\right)^n$	0.73	2.086	[4]
	0.78	2.177	[9]
	0.30	1.36	[30]
	0.73	2.068	[35]
	0.75	2.98	[41]
	0.3	1.5	[32]
	0.59	1.7	[33]
	0.506	2.7	Present study with SR 1.0
	0.506	2.79	Present study with SR 0.1
	0.506	2.95	Present study with SR 0.01
$E_f = c_e * E_d (\rho_{rd})^{ne}$	0.735	1.654	[17]
	1.96	2.73	[9]
	0.196	1.43	[31]
	1.59	4.72	[20]
	1.0	2.96	[30]
	3.12	3.80	Present study with SR 1.0
	2.16	3.95	Present study with SR 0.1
	1.75	4.05	Present study with SR 0.01
$\varepsilon_d = C_d - n_d \rho_{rd}$	1.36	1.57	[4]
	1.80	2.45	[9]
	2.4	2.54	[16]
	0.719	0.302	Present study with SR 1.0
	0.716	0.325	Present study with SR 0.1
	0.713	0.348	Present study with SR 0.01

Table 4: The value of empirical constants reported by various researchers and that obtained in the present study for different empirical relations.

be written in term strain rate and relative density. As shown through Eq. (5).

$$\sigma_{pl} = 0.5063 \times (733.91)\ \dot{\varepsilon}^{0.0779} \times (\rho_{rd})^{2.6958-0.0531\ln(\varepsilon)} \quad (5)$$

The strain rate sensitivity of dense Ti_6Al alloy is noted to be 0.0779, which is relatively higher than that of Al-alloy [35] at room temperature. In order to determine the strain rate sensitivity of Ti_6Al foams, ln (σ_{pl}) is plotted as a function of ln ($\dot{\varepsilon}$) in Figure 10. The slope of the line 'm' termed as strain rate sensitivity. It is noted that 'm' is varying in the range of 0.104 to 0.127 (Figure 10). It indicated that the strain rate sensitivity of Ti_6Al foam is marginally higher than that of dense Ti_6Al. This also signifies that Ti_6Al foams are relatively more strain rate sensitive as compared to Al foams (0.03 to 0.05) in room temperature [35]. Figure 11a depicts that the strengthening coefficient 'k' increases with increases in RD and follows the linear relationship. This is due to the fact that the solid fraction responsible for deformation increases with increase in RD. Because of thicker cell wall, cell wall bending and shearing get resisted to a greater extent. This is also another reason for lower 'm' in foam materials. Figure 11b shows that 'm' decreases linearly with RD. The dense Ti_6Al also exhibited 'm' to be 0.0779. As RD increases, the foam becomes denser and m decreases. The plateau stress thus can also be expressed in term of strain rate and relative density by the following relation as stated in equation (6).

$$\sigma_{pl} = (159.4\rho_{rd} - 32.851)\ \dot{\varepsilon}^{(0.1567-0.1162\rho rd)} \quad (6)$$

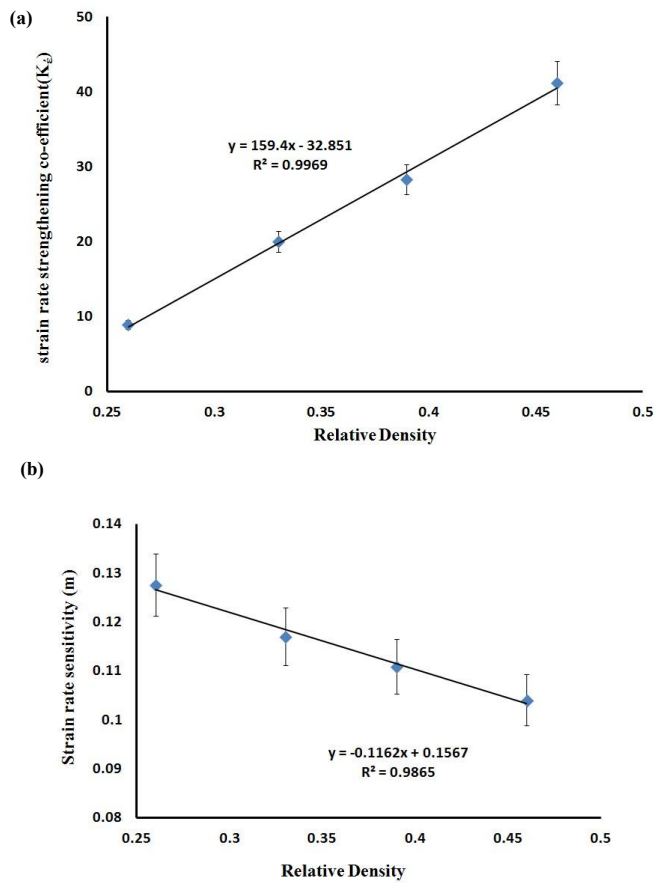

Figure 11: (a) Strain rate strengthening co-efficient (K_ε) {of the ln (σ_{pl}) (verse ln ($\dot{\varepsilon}$)} vs. relative density. (b) Strain rate sensitivity (m) {slop of the ln (σ_{pl}) verse ln ($\dot{\varepsilon}$)} vs. relative density.

Young's modulus

The Young's modulus (E_f) of Ti_6Al alloy foam as a function of RD under different strain rates is shown in Figure 12. The Young's modulus also follows the similar trend with relative density to that observed for plateau stress. In the present study, for similar relative density the plateau stress increases with increase in the strain rate**.** The Young's modulus of these foams as a function of relative density can be expressed through the following type of relation:

$$E_f = c_e \times E_d (\rho_{rd})^{n}_{e} \quad (7)$$

Where E_d is the Young's modulus of dense Ti_6Al alloy, C_e and n_e are the proportionality constant and exponent respectively and ρ_{rd} is the relative density of foam. Here the Young's modulus of dense Ti_6Al alloy (E_d) is measured to be 120 ± 10 GPa. The Young's modulus of dense material is noted to be almost invariant to the strain rate. The best fitted relations indicate that the proportionality constant increases with increase in strain rate, whereas the exponent decreases with strain rate. The proportionality constant and the exponent of the above equation vary with strain rate. These individual equations are reported within Figure 12. The constants are compared with the reported values in Table 4. These values are in good agreement with reported values. Thus, these results demonstrate that the modulus obtain in the synthesized foam are in close agreement with reported value. Through best fitting approach of proportionality constant (c_e) and exponent (n_e) with the strain rate ($\dot{\varepsilon}$), the Young's modulus (E_f) of these Ti_6Al foams can be expressed as a function of strain rate and ρ_{rd} through following relations:

$$E_f = (0.2968 \ln(\dot{\varepsilon}) + 3.1781) \times E_d (\rho_{rd})^{-0.0553 \ln(\dot{\varepsilon}) + 3.8122} \quad (8)$$

But the Young's modulus of the foams is found to be increased with increase in strain rate when the difference in Young's modulus is noted to be significantly higher at higher RD. This may be due to the fact that sintering is carried out at relatively lower temperature and there exit significant amount of inter-particles porosities. Particles are bonded at localized region. As a result, the stress distribution within the cell wall is greatly influenced by these pores. The load transfer along the cell wall may not be effective. At higher relative density the degree of particle fusion is higher and thus lead to more effect load transfer. This may be one of the causes of significant differences in modulus at higher RD. However, detailed studies are required on these foams after sintering at

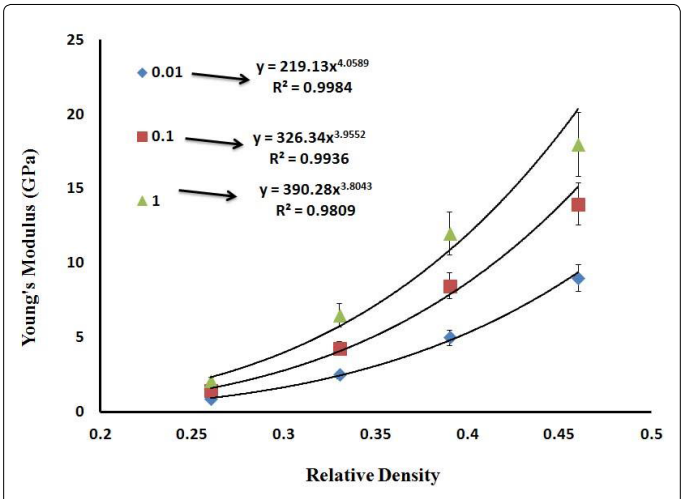

Figure 12: Variation of Young's modulus of Ti_6Al alloy foam samples with different relative density.

higher different temperatures for larger deformation. These studies are in progress will be communicated later as separate paper.

Stress drop

The stress is the measure of the reduction in stress from its peak stress (plastic collapse stress (σ_{pc})) to the average plateau value (σ_{p1}), the stress drop ($\Delta\sigma$) can be written as (σ_{pc}-σ_{p1}). The stress drop ratio is the normalized stress drop with respect to the σ_{p1} and defined as the ratio of $\Delta\sigma$ to σ_{p1}. It may be noted that stress drop ratio ($\Delta\sigma/\sigma_{p1}$) decreases with increase in RD. This is primarily due to the fact that at lower RD, the stress or impulse wave propagation in the foam reduces and more strain localization takes place. The cell walls bending, and shearing are the prevailing deformation mechanism in foam. Because of the possibility of greater stress or strain localization, the cell wall crashed to greater extent. The micro-porosity in cell wall is higher due to localized bonding between particles during sintering for lower RD. This further facilitates cell wall crashing and reduction in stress after plastic collapse stress to a greater extent. The cell wall hardening is reduced. This could also be observed from the stress strain curves. In case of higher relative density, the cell walls are thicker and thus possibility of cell wall bending and shearing took place relatively gradually and slowly with respect to the strain. Again, at higher relative density, the cell wall matrix hardened to a greater extent. For example, the microhardness of the cell wall of foam with 0.26 RD is 240 HV, whereas that of foam with 0.46 RD is 260 HV after deformation. Prior to the deformation, the micro-hardness of foams was 230 HV and 235 HV for 0.26 and 0.46 RD respectively. Greater extent of cell wall hardening as well as shearing are take place. Because of greater extent of cell wall shearing, cell wall cracking increases. But because of thicker cell wall and also more effective bonding between particles, the stress reduced gradually. The probability of cell wall shearing with respect to the overall cell wall fraction is reduced. This causes lower value of stress drop ratio. However, if the absolute value of stress drop is considered, the trend is reversed. Because of lower relative density, the number of cells gets crushed at a given strain is less. The reverse is true for higher density. At lower relative density, the stress drop is reduced. These could also be realized from the deformed sample of Ti_6Al foam with RD = 0.26 and 0.46. When RD is low, samples are compacted with fewer cracks. But the foam with higher density gets fragmented more severely during compaction.

Densification strain

The densification strain (ε_d) of the Ti alloy foam is a function of relative density when tested at different strain rates is shown in Figure 13. It is evident from this Figure that ε_d decreases with increase in relative density following a linear relationship. From Table 3 it is noted that densification strain increased very marginally with the strain rate. There is only 2% to 3% variation in densification strain when the strain rate changes from 0.01/s to 1.0/s. For example, in case of relative density 0.26, the value of ε_d is found to be 0.62, 0.63 and 0.64 at strain rate of 0.01/s, 0.1/s and 1.0/s respectively. This is due to the fact that ε_d signifies the extant of consolidation of pores during deformation, which primarily be governed by the extent of porosity exists within the foam. Similar kind of trend also follows with other relative densities. The ε_d as a function of relative density can be expressed with following type of relation.

$$\varepsilon_d = C_d - n_d \rho_{rd} \quad (9)$$

It is evident from this plot that both 'C_d' and 'n_d' varies in narrow range. 'C_d' varies 0.713 to 0.719 and "n_d" varies in the range 0.302 to 0.348. This clearly signifies that densification strain is almost invariant to the strain rate. Thus, the general relation between ε_d and RD can be expressed as follows:

$$\varepsilon_d = -0.3257 - 0.716\rho_{rd} \quad (10)$$

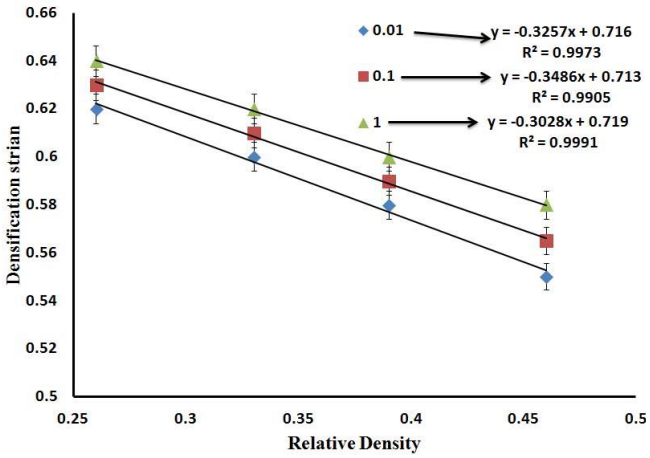

Figure 13: Variation of the densification strain (ε_d) with relative density at different strain rates.

Energy absorption (E_{ab})

The energy absorption of the foam is defined as the area under the stress-strain curve up to the densification strain. In the present study, energy absorption capacity of Ti_6Al alloy foam is calculated from the stress strain curve up to 0.5% strain deformation by using standard methodology [29].

$$E_{ab} = \int_o^{\varepsilon d} \sigma d\varepsilon \quad (11)$$

Where, ε_d = densification starin, σ =Stress, ε= Strain. Variation of energy absorption of Ti_6Al alloy foam as a function of relative density with different strain rates is shown in Figure 14. It is clear from this Figure that E_{ab} increases with increase in relative density following a power law relationship. The relationship between E_{ab} and RD are similar type of the relation to that between σ_{p1} and relative density. This signifies that E_{ab} is primarily governed by σ_{p1} and the energy absorption of these foam increases with increase in the relative density and the strain rate. The power law relationships are shown within the Figure. The proportionality constants and the exponents of these relations are best fitted with strain rate (Figure 15) and finally the relationship amongst E_{ab}, $\dot{\varepsilon}$ and relative density (ρ_{rd}) can be written in the following way:

$$E_{ab} = (6.0087\ 1n\ (\varepsilon) + 118.26) \times (\rho_{rd})^{2.3554-0.06151n\ (\varepsilon)} \quad (12)$$

Figure 16 shows the relationship between ln (E_{ab}) and ln ($\dot{\varepsilon}$) for different ρ_{rd}. The slope of line ($m_{Eb\varepsilon}$)termed as the strain rate energy sensitivity and constant ($K_{Eb\varepsilon}$) is termed as the strain rate energy absorption capacity. The m_{Eb} and $K_{Eb\varepsilon}$ of the equations in Figure 17 are best fitted with relative density and the other form of relationship amongst energy absorption (E_{ab}), relative density (ρ_{rd}), and strain rate ($\dot{\varepsilon}$) are observed which is shown below:

$$E_{ab} = (28.979\rho_{rd} - 2.2027) \times \varepsilon^{0.1832-0.1933\rho rd} \quad (13)$$

The value of (m_{Eb}) decrease in the range of 0.131 to 0.094 with relative density and follow a linear relationship. It is noted that the

strain rate energy absorption coefficient (K_{Ebe}) increases with ρ_{rd} and also follows a linear relationship. It may be noted that the strain rate sensitivity of these Ti_6Al foams are marginally higher than those of aluminum foams. This may be due to the marginally higher strain rate sensitivity of dense Ti_6Al alloy as compared to that of dense aluminum alloy (Table 5) [35].

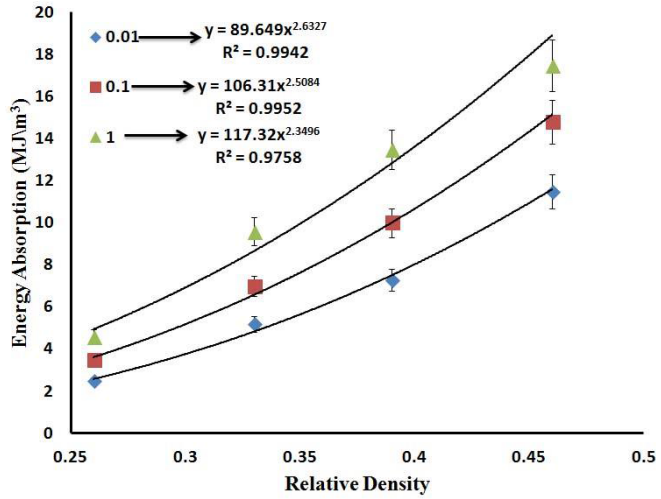

Figure 14: Variation of energy absorption (E_{ab}) with relative density at different strain rates.

Strain rate sensitivity parameter

The strain rate plays important role for compression deformation in the quasi- static and dynamic state. The strain rate sensitivity parameter signifies the influence of strain rate on the plateau stress or plastic collapse stress as compared to that in static condition. The strain rate sensitivity parameter (Σ) of Ti-Al foam is calculated by using following relationship [35-39].

$$\sum = \frac{\sigma d - \sigma q}{\sigma *} * \left(\frac{1}{1n\left(\frac{\varepsilon d}{\varepsilon q}\right)} \right) \quad (14)$$

Where σ* is the stress at 5% stain, σ_q is quasi-static stress at 0.001/s strain rate, $\dot{\varepsilon}$ is strain rate and σ_q is the peak stress at any strain rate. Thus, at strain rate 0.001/s, 'Σ' is zero. The foam shows abrupt variation in stress during compressions which are not seen, generally, in dense

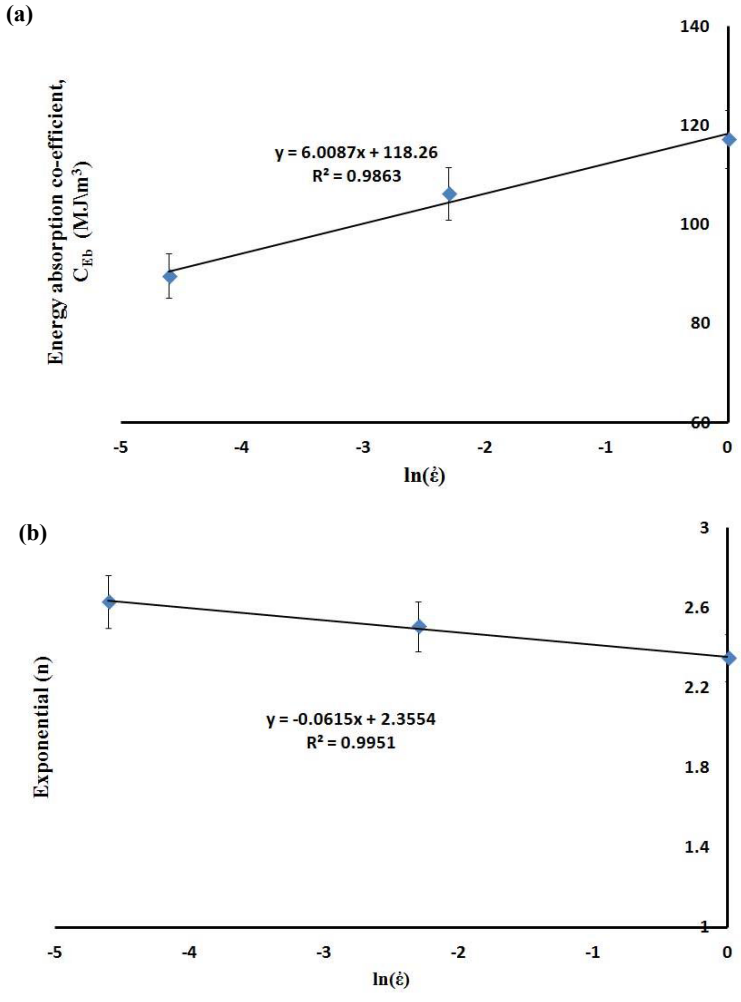

Figure 15: Variation of (a) energy absorption co-efficient (C_{Eb}) verse ln ($\dot{\varepsilon}$). (b) Exponential (n) {of the E_{ab} vs RD} verse ln ($\dot{\varepsilon}$).

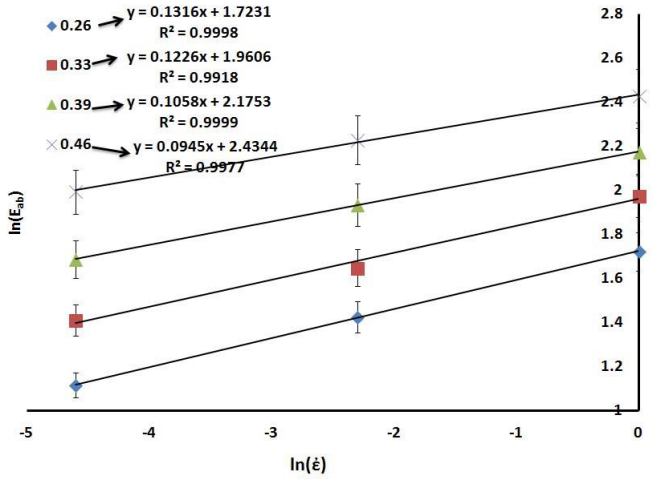

Figure 16: Variation of ln (E_{ab}) verse ln ($\dot{\varepsilon}$)

material and composite metal. The different stress values in static and quasi static condition and resulting strain rate sensitivity parameter are summarized in Table 3. The sensitivity parameter is varied in the range of 0.034 to 0.078 which is marginally higher than that of the aluminum matrix as reported in Table 5. The different values of the sensitivity parameter are due to the fact that the deformation behaviour are dependent on volume fraction of pores, cell size, cell wall thickness and the nature of base material. The particle bonding and inter particle porosities also affect the strain rate sensitivity parameter. These require in depth study as stated earlier and these studies also to be carried out at very high strain rate (i. under dynamic condition). These studies are in progress which again will be communicated later.

Conclusions

The following conclusions can be drawn from the present study:

1. Elemental metal powder can be used for making Ti-Al alloy foams. The ammonium bicarbonate particles can be used as space holder for making Ti_6Al.

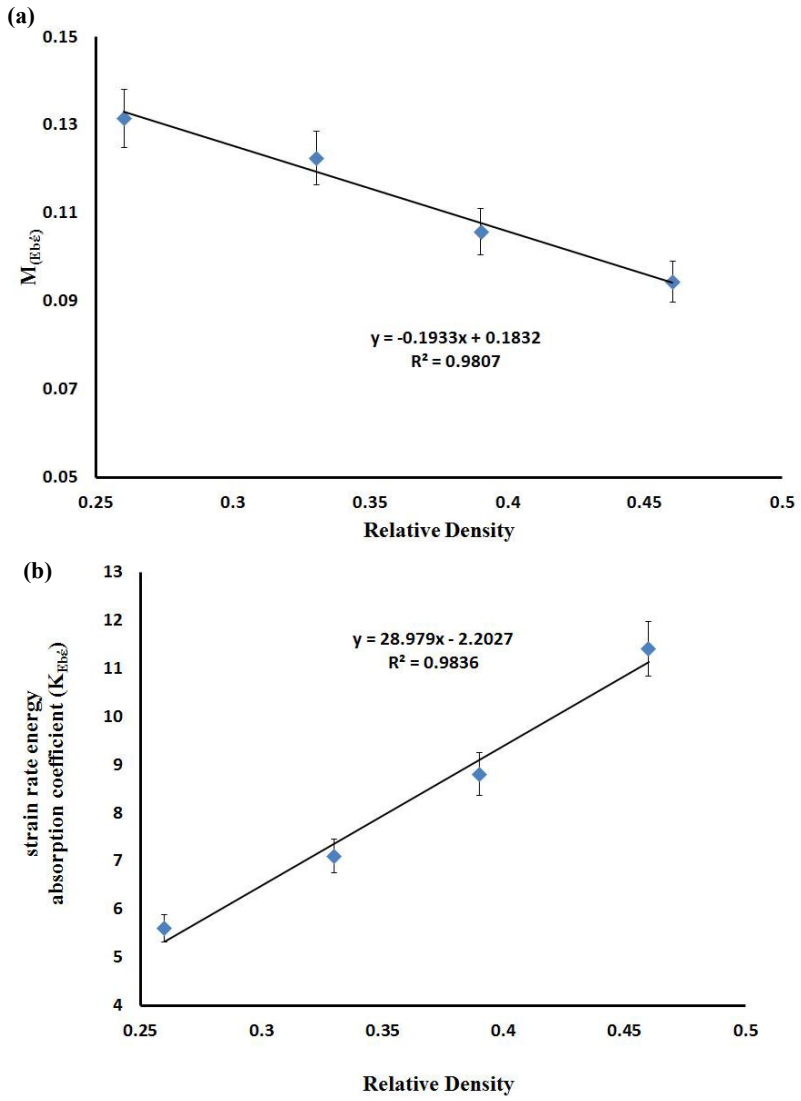

Figure 17: Variation of (a) m_Ebε̇ {slop of ln (E_{ab}) (verse ln ($\dot{\varepsilon}$)}verse relative density. (b) Strain rate energy absorption capacity ($K_{Ebε̇}$) vs relative density.

Formulae	Strain rate sensitivity parameter	Foam matrix	References
$\sum \frac{\sigma_d - \sigma_q}{\sigma^*} \left(\frac{1}{\ln\left(\frac{\varepsilon'_d}{\varepsilon'_q}\right)} \right)$	0.028-0.063	Al-cenosphere syntactic foam.	[35]
	0.01-0.07	Al- matrix syntactic foam.	[38]
	0.01-0.06	Al- reinforced aluminum composite.	[39]
	0.04-0.08	Ti_6Al foam.	Present study

Table 5: The value of strain rate sensitivity parameter reported by various researchers and that obtained in the present study.

2. The foam density can be controlled by controlling the space holder content in green compact. The cell size of foam will be also be controlled by controlling the size of space holder.

3. The green compact should be sintered in three stages to avoid removal of Al without solid state diffusion. During sintering greater extent of shrinkage is noted after final stage of sintering indicating solid state fusion during this stage.

4. Because of solid state fusion the cell size become marginally lower than that of average space holder size. This also causes nullification of fraction inter particle pores during sintering causes marginal decrease in porosity as compared that before sintering.

5. The plateau stress, energy absorption of these foams is following power law relationship with relative density. However, the densification strains following linear relationship with relative density.

6. The stress drop ratio decreases with increase in relative density and strain rate. This is due to less probability of individual of cell wall crushing under these conditions. But overall cell wall shearing and crushing increased with increased in strain rate relative density, which is why the absolute stress drop increases with strain rate and relative density.

7. The strain rate sensitivity is low irrespective of relative density but when compared with reported values in aluminum foams, this is relatively at higher range. This indicates Ti foams are relatively more strain rate sensitive to that of Al foams. This might be of higher strain rate sensitivity of dense Ti as compared to the Al alloys.

8. The strain rate sensitivity parameter marginally decreases with increase in relative density. This also validates the observation and strain rate sensitivity of dense Ti to be lower than that of foam. Strain rate sensitivity parameter is almost invariant to relative density but increases substantially with increase in strain rate.

9. The plateau stress, densification strain, and energy absorption have empirically correlative with relative density and strain rate. The coefficient and exponent in the present study are good agreement with reported value.

Conflict of Interest

The authors declare that they have no conflict of interest.

References

1. García I, Gracia-Escosa E, Bayod M, Conde A, Arenas A, et al. (2016) Sustainable production of titanium foams for biomedical applications by concentrated solar energy sintering. Mater Lett.
2. Salimon A, Brechet Y, Ashby MF, Greer AL (2005) Potential application of steel and titanium metal foams. J mater sci 40: 5793-5799.
3. Spoerke ED, Murray NG, Li H, Brinson LC, Dunand DC, et al. (2005) A bioactive titanium foam scaffold for bone repair. Acta Biomater 1: 523-533
4. Guo WY, Sun J, Wu JS (2009) Electrochemical and XPS studies of corrosion behavior of $Ti_{23}Nb$-0.7Ta_{27}r-O alloyed in ringer's solution. Mater Chem and Phy 113: 816-820.
5. Ik-Hyun O, Naoyuki N, Naoya M, Shuji H (2003) Mechanical properties of porous titanium compacts prepared by powder sintering. Scripta Mater 49: 1197-1102.
6. Jing L, Hailin Y, Huifeng W, Jianming R (2014) Low elastic modulus titanium-nickel scaffolds for bone implants. Mater Sci Eng C 34: 110-114.
7. karageorgiou V, Kaplan D (2005) Porosity of 3D biomaterial scaffolds and osteogenesis. Biomaterials 26: 5474-5491.
8. Jurczyk MU, Jurczyk K, Miklaszewski A, Jurczky M (2011) Nanostructured titanium-45S5 bio-glass scaffold composites for medical applications. Mater Des 32: 4882-4889.
9. Mondal DP, Patel M, Jain H, Jha AK, Das S, et al. (2015) The effect of the particle shape and strain rate on microstructure and compressive deformation response of pure Ti-foam made using acrowax as space holder. Mater Sci Eng A 625: 331-342.
10. Oshida Y (2007) Bioscience and bioengineering of titanium materials. (2nd edn) Elsevier, Great Britain.
11. Piszek P, Muchewicz Z, Radtke A, Gryglas M, Dahm H, et al. (2013) CVD of TiO_2/Ag antimicrobial layer deposition from the hexanuclear muoxo Ti (iv) complex as a precursor, and the characterization. Surf Coat Int 222: 38-43.
12. Wagner J, Edlmayr V, Penoy M, Michotte C, Kathrein M (2008) Deposition of Ti-Al-N coating by thermal CVD. Int J Refract Met Hard Mater 26: 563-568.
13. Clemow AJ, Weinstein AM, Klawitter JJ, Koeneman J, Anderson J (1981) Interface mechanics of porous titanium implants. Biomed Mater Res 15: 73-82.
14. Murray NGD, Dunand DC (2003) Microstructure evolution during solid-state foaming of titanium. Compos Sci Technol 63: 2311-2316.
15. Li JP, Li SH, Blitterswijk CA, Van P, De Groot K (2005) A novel porous Ti_6Al4V: Characterization and cell attachment. J Biomed Mater Res 73A: 223-233.
16. Mondal DP, Patel M, Das S, Jha AK, Jain H, et al. (2014) Titanium foam with coarser cell size and wide range of porosity using different types of evaporative space holders through powder metallurgy route. Mater Des 63: 89-99.
17. Nidhi J, Mondal DP, Majumdar JD, Anshul B, Jha AK, et al. (2013) Highly porous open cell Ti-foam using NaCl as temporary space holder through powder metallurgy route. Mater Des 47: 810-819.
18. Jakubowicz J, Adamek G, Dewidar M (2013) Titanium foam made with saccharose as a space holder. J Porous Mater 20: 1134-1141.
19. Nihan T, Gursoy A (2009) Designing compressive properties of titanium foams. J Mater Sci 44: 1477-1484.
20. Esen Z, Bor S (2007) Processing of Ti foam using magnesium space particle. Scripta Mater 56: 341-344.
21. Mondal DP, Hament J, Das S, Jha AK (2015) Stainless steel foams made through powder metallurgy route using NH_4HCO_3 as space holder. Mater Des 88: 430-437.
22. Aguilar C, Guerra C, Lascano S, Guzman D, Rojas PA, et al. (2016) Synthesis and characterization of Ti-Ta-Nb-Mn foams. Mater Sci Eng C 58: 420-431.
23. Ezgi B, Ziya E, Sakir B (2015) *In vitro* bioactivity investigation of alkali treated Ti_6Al7Nb alloy foams. Appl Surf Sci 327: 437-443.
24. Erkan AE, Şakir BOR (2015) Fatigue behavior of Ti-6Al-4V foams processed by magnesium space holder technique. Mater Sci Eng A 621: 157-165.
25. İpek NG, Dericioğlu F Arcan P, Şakir B (2013) Monotonic and cyclic compressive behavior of superelastic TiNi foams processed by sintering using magnesium space holder technique. Mater Sci Eng A 582: 140-146.

26. Munoz S, Pavon J, Rodrıguez-Ortiz J, Civantos A, Allain JP, et al. (2015) On the influence of space holder in the development of porous titanium implants: Mechanical, computational and biological evaluation. Mater Charact 108: 68-78.

27. Zhuravleva K, Bönisch M, Scudino S, Calin M, Schultz L, et al. (2014) Phase transformations in ball-milled Ti–40Nb and Ti–45Nb powders upon quenching from the ß-phase region. Powder Technol 253: 166-171.

28. Xiang C, Yan Z, Zengfeng L, Hanliang Z, Huang Y, et al. (2012) Preparation and compressive behavior of porous titanium prepared by space holder sintering process. Proc Eng 27: 768-774.

29. Mondal DP, Majumdar DJ, Jha N, Badkul A, Das S, et al. (2012) Titanium-cenosphere syntactic foam made through powder metallurgy route. Mater Des 34: 82-89.

30. Mansourighasri A, Muhamad N, Sulong AB (2012) Processing titanium foams using tapioca starch as a space holder. J Mater Proc Tech 212: 83-89.

31. Niu W, Bai C, Qiu G, Wang Q (2009) Processing and properties of porous titanium using space holder technique. Mater Sci Eng A 506: 148-151.

32. Andrews E, Sanders W, Gidson LJ (1999) Compressive and tensile behaviour of aluminium foams. Mater Sci Eng A 270: 113-124.

33. Jianhu S, Guoxing L, Dong R (2011) Compressive behaviour of closed cell aluminum foams at high strain rate. Compos Part B 41: 678-685.

34. Gibson LG, Ashby MF (1997) Cellular solids: Structures and properties (2nd edn) Cambridge University Press. Cambridge, UK.

35. Goel MD, Mondal DP, Yadav MS, Gupta SK (2014) Effect of strain rate and relative density on compressive deformation behavior of aluminum cenosphere syntactic foam. Mater Sci Eng A 590: 406-415.

36. Balch DK, O'Dwyer JG, Davis GR, Cady CM, Gray GT, et al. (2005) Plasticity and damage in aluminum syntactic foams deformed under dynamic and quasi-static conditions. Mater Sci Eng A 391: 408-417.

37. Dou ZY, Jiang LT, Wu GH, Zhang Q, Xiu ZY, et al. (2007) High strain rate compression of cenosphere-pure aluminum syntactic foams. Scripta Mater 57: 945-948.

38. Myers K, katona B, Cortes P, Orbulov IN (2015) Quasi-static and high strain rate response of aluminum matrix syntactic foams under compression. Compos Part A 79: 82-91.

39. San MC, Fahe C, Kouzeli M, Mortensen A (2002) Quasistatic and dynamic compression of aluminum-oxide particle reinforced pure aluminum. Mater Sci Eng A 337: 202-211.